

Assignments of the Two-Phonon Infrared Absorption Spectrum of LiF[†]

J. E. Eldridge

Department of Physics, The University of British Columbia, Vancouver, British Columbia, Canada

(Received 20 December 1971)

Measurements of the far-infrared lattice absorption in LiF at several temperatures are reported. An approximate calculation of the relative two-phonon absorption intensity has been made considering the anharmonic mechanism only and using the lattice-dynamical data, resulting from a modified deformation-dipole model, of Karo and Hardy. The wave-vector density used was 64 000 points per zone (1685 independent wave-vector positions). Such a density with a simple bin-sampling smoothing procedure gave a fairly good wave-number resolution in the computed two-phonon spectra. The agreement with the two-phonon difference absorption presented here and the summation results reported elsewhere is poor, but the discrepancies may be seen to be in the lattice-dynamical data. By identifying the phonon branches responsible for the features in the computed spectrum and considering various criteria necessary for strongly combining branches, it was possible to take the more accurate frequencies recently measured by inelastic neutron scattering and satisfactorily explain the experimental features. Phonon branches of less symmetry than the three major branches were found to contribute appreciably. No evidence was found for sizeable three-phonon absorption in the far infrared.

I. INTRODUCTION

The lattice absorption of electromagnetic radiation in alkali halide crystals extends from the far infrared to the near infrared. In the midrange there is very strong one-phonon "reststrahlen" absorption, accompanied by high reflection, corresponding to the resonant interaction with the degenerate transverse optical modes. At lower energy there occurs strongly temperature-dependent absorption, normally attributed to two-phonon difference processes, while at higher energy are seen the less-temperature-dependent multiphonon (mainly two-phonon) summation processes. These effects may be examined by absorption or reflection measurements, or a combination of both. A good example of a standard reflectivity analysis is that of Gottlieb,¹ who obtained real and imaginary parts of the dielectric constant and refractive index for LiF from a Kramers-Kronig analysis. Direct absorption measurements of the reststrahlen and summation bands of LiF, using a wide range of crystal thicknesses, have also been made by Karo, Hardy, Smart, and Wilkinson² (this reference will hereafter be referred to as I). Recently the technique of asymmetric Fourier spectroscopy has been used by Johnson and Bell³ to yield more accurate optical constants for KCl and KBr.

The mechanisms for the reststrahlen peak broadening and the two-phonon sidebands are known to be the higher-order (anharmonic) terms in the lattice potential energy and the nonlinear terms in the electric dipole moment. The latter is the sole mechanism for similar sidebands in nonpolar compounds where no resonance exists. In alkali ha-

lides the anharmonic terms have usually been assumed the predominant mechanism for the sidebands at least in the vicinity of the main peak. Szigeti⁴ in 1960, however, treated both mechanisms in a systematic way and predicated that far from resonance the second moment may play a large role. Cowley⁵ also considered both mechanisms, and computed theoretical optical constants for NaI and KBr using shell-model dispersion curves fitted to neutron data. The dipole-moment contribution was predicted to be small. No good experimental data existed, however, for comparison. Mitskevich⁶ performed a similar analysis for LiF and MgO and compared it with some success with early experimental data which was not, however, as accurate as obtained in I. The effect of the second moment on the theoretical summation bands was again small.

With the publication of the results of a fairly successful deformation-dipole model analysis of the lattice dynamics of alkali halides by Karo and Hardy,⁷ it became possible to attempt a simplified interpretation of the structure of summation bands merely in terms of peaks in the combined density of states, resulting from critical points, usually found near the zone boundary. Karo and Hardy themselves in I showed that the frequencies of the few features seen in the optical summation bands of LiF agreed reasonably with the peaks in such a combined density of states resulting from a wave-vector density of 1000 points per Brillouin zone. This technique had been successfully applied to zinc-blende-type semiconductors⁸ and diamond⁹ (for a recent review see Ref. 10), but in these crystals a far greater number of symmetry com-

binations are allowed. However, with the availability of the eigenvectors and eigenvalues from these models, kindly supplied by Karo, it became possible to make a quantitative theoretical comparison with experiment, using appropriate theory like Cowley's⁵ to couple the various phonon pairs, but without having to generate neutron-fitting data. Ipatova, Maradudin, and Wallis¹¹ used this data with a density of 8000 wave vectors per zone, and their own theory which included anharmonic terms only, to calculate the optical properties of NaCl and LiF. The LiF results in the summation region showed too much structure, which they attributed to the coarse grid of wave vectors, and some large differences in magnitude from the experimental results. No attempt was made to identify the phonon pairs responsible for any features. Johnson and Bell,³ also neglecting nonlinear moments, and using Karo and Hardy's data for KCl with a density of 1000 wave vectors per zone found fair agreement with experiment but some large errors in magnitude. They attempt to identify the summation features in terms of combinations of peaks in the one-phonon density of states, which is inappropriate since the combining phonons must have equal but opposite wave vectors. Their experimental curve for KBr also differed appreciably from the theory of Cowley.⁵

Recently Dolling *et al.*¹² measured the dispersion curves of LiF at room temperature by inelastic-neutron-scattering techniques. They show that errors have been made in previous assignments of multiphonon sidebands to electronic transitions. They also show from their combined density-of-states curve and with the help of selection rules derived from group-theoretical arguments of Burstein *et al.*,¹³ that there remains considerable ambiguity in the peak assignments of the optical summation measurements of I. This is due to the fact that their combined density-of-states curve had such good frequency resolution that it showed many more features than had been obtained in I from a wave-vector grid of 1000 per zone or had been seen optically. Group theory shows that some of the strong combinations are forbidden (e.g., all pairs at X), but only by applying the appropriate theory in a manner similar to Refs. 3, 5, or 11, and thus incorporating the coefficients which couple the various modes, can an unambiguous assignment of the peaks be made. A high wave-vector density with appropriate smoothing technique is also required if the fine structure is to be resolved and noise in the theoretical spectrum avoided.

It was the original intention of this paper to report and identify the features of the far-infrared absorption in LiF, measured at various temperatures. Any deviation in intensity between experiment and theory as the temperature was raised

would indicate contributions, which Stolen and Dransfield¹⁴ maintain are appreciable (see also Hadni¹⁵), from three-phonon or multiphonon processes. An approximate calculation similar to Ref. 3 has therefore been made of the two-phonon difference absorption, including the anharmonic mechanism only and using the lattice-dynamical data of Karo and Hardy, with a wave-vector density of 64 000 points per Brillouin zone (1685 independent wave-vector coordinates in the irreducible $\frac{1}{48}$ th of the zone). This gave a resolution of a few wave numbers. The calculated temperature dependence will be seen to agree well with experiment, indicating no need to consider higher-order processes in this case, but the calculation will also be seen to predict none of the features observed in the far-infrared spectrum. It was therefore extended to cover the two-phonon summation processes measured in I in the near infrared, in an effort to predict the features previously mentioned. Once again the comparison will be seen to be poor, indicating possibly some discrepancies in the lattice-dynamical data. Indeed, upon inspection the frequencies predicted by the refined deformation-dipole model of Karo and Hardy may be seen to differ, appreciably in some regions, from the more accurate inelastic-neutron-scattering measurements. Nevertheless, by identifying the phonon branches responsible for the features in the computed spectrum and by also considering three or four criteria, implicit in the theory, which determine the possible strong combinations (summation or difference), it has been possible to satisfactorily explain the experiment data both above and below the reststrahlen frequency with the aid of the accurate neutron frequencies.

II. EXPERIMENT

The crystals used were natural LiF supplied by Harshaw Chemical Company. They were cut with a diamond saw, then mechanically polished with alumina on a nylon cloth, the final alumina size being 0.3 m μ . This was followed by ultrasonic cleaning. The final size was approximately 1 \times 2.5 cm with a thickness varying from 0.02 to 0.1 cm. The samples were slightly wedge shaped to avoid interference effects.

The measurements were performed on a Beckman model No. FS720 far-infrared Fourier spectrophotometer, with a step drive and Golay detector. This latter was the main limitation on the signal-to-noise ratio. A typical run was two hours for a double-sided interferogram and a resolution between 5 and 10 cm⁻¹. The low-temperature measurements were obtained by clamping the samples, with silver grease, to a rotatable cold finger of a metal Dewar containing liquid nitrogen. This was pumped to give the 63 \pm 2 °K data.

III. THEORY

The theory is taken from Johnson and Bell³ who

$$\chi_{\alpha}(\omega) = \chi_{\alpha}^E + \frac{1}{Nv\hbar} \sum_j \frac{2\omega(0,j)M_{\alpha}^2(0,j)}{\omega^2(0,j) - \omega^2 + 2\omega(0,j)[\Delta(0,j;\omega) - i\Gamma(0,j;\omega)]}, \quad (1)$$

where χ_{α}^E is the electronic contribution, N the number of unit cells in the crystal, v the volume of the LiF unit cell, and $\omega(0,j)$ the angular frequency of the zero-wave-vector phonon with branch index j . $M_{\alpha}(0,j)$ is the first-order dipole-moment coefficient in the α direction. $\Delta(0,j;\omega)$ and $\Gamma(0,j;\omega)$ are the Hermitian and anti-Hermitian parts of the proper self-energy matrix, arising from lattice anharmonicity.

Since comparison is to be made with the conductivity $2\sigma(\text{cm}^{-1})$ plotted in I over the summation re-

considered only the third-order anharmonicity and neglected the second-order electric moment. The dielectric susceptibility is then given by

gion, and $\sigma = nk\bar{v}$ where n is the real part of the refractive index, k the extinction coefficient and $\bar{v} (= \omega/2\pi c)$, the wave number in cm^{-1} , then what is required from Eq. (1) is the imaginary part of the dielectric constant ϵ'' (equal to $2nk$) times the wave number. The comparison with the difference region measured here will require α (equal to $4\pi k\bar{v} = 4\pi\sigma/n$) so that in the region the classical form for n given by Eq. (11) may be used. Thus the real part of Eq. (1) will not be calculated and the reststrahlen peak ignored. With $\epsilon = 1 + 4\pi\chi$,

$$\sigma(\omega) = \frac{4\omega}{Nv\hbar c} \frac{\omega^2(0,j)M_{\alpha}^2(0,j)\Gamma(0,j;\omega)}{[\omega^2(0,j) - \omega^2 + 2\omega(0,j)\Delta(0,j;\omega)]^2 + 4\omega^2(0,j)\Gamma^2(0,j;\omega)}. \quad (2)$$

The summation over j has been removed since only the degenerate transverse optical modes at $\vec{k} = 0$ will be involved. Further, since the features and not the magnitude of the two-phonon spectra are of concern, $\sigma(\omega)$ will not be calculated absolutely but will be scaled by fitting the difference spectra. The following approximations will now be made. The last term in the denominator is important only at frequencies very close to the resonant frequency (i. e., under the reststrahlen peak) and will therefore be ignored. Secondly, in the denominator, $\omega^2(0,j) + 2\omega(0,j)\Delta(0,j;\omega)$ is put equal to ω_T^2 , the resonant frequency found from thin-film transmission measurements¹⁸ at 2 and 290 °K and found in Table I. This is a more serious approximation than the first as may be judged by the relative magnitudes of $\omega(0,j)$ and $\Delta(0,j;\omega)$ calculated³ for KCl. Furthermore $\Delta(0,j;\omega)$ has a strong frequency dependence which will affect the structure of the phonon combination bands. However, since both $\Delta(0,j;\omega)$ and $\Gamma(0,j;\omega)$ exhibit similar structure, arising from their dependence on the third-order anharmonic coupling coefficient, the second approximation above should still allow unambiguous two-phonon assignments of the measured peaks. Thus

$$\sigma \propto \omega\Gamma(0,j;\omega)/(\omega_T^2 - \omega^2)^2. \quad (3)$$

An expression for $\Gamma(0,j;\omega)$ is given³ as

$$\Gamma(0,j;\omega) = \frac{18\pi}{\hbar^2} \times \sum_{\vec{k}_1, j_1} \sum_{\vec{k}_2, j_2} |V^{(3)}(0,j;\vec{k}_1, j_1; \vec{k}_2, j_2)|^2 S(\omega), \quad (4)$$

where

$$S(\omega) = [n(\vec{k}_1, j_1) + n(\vec{k}_2, j_2) + 1] \times \delta(\omega - \omega(\vec{k}_1, j_1) - \omega(\vec{k}_2, j_2)) \quad (5a)$$

for the summation bands,

$$S(\omega) = [n(\vec{k}_1, j_1) - n(\vec{k}_2, j_2)] \times \delta(\omega + \omega(\vec{k}_1, j_1) - \omega(\vec{k}_2, j_2)) \quad (5b)$$

for the difference bands, and

$$n(\vec{k}, j) = [e^{\hbar\omega(\vec{k}, j)/k_B T} - 1]^{-1}, \quad (6)$$

the Bose-Einstein occupation number. \vec{k} is the phonon wave vector equal to the reciprocal of the wavelength.

The third-order anharmonic coefficient $V^{(3)}(0,j;\vec{k}_1, j_1; \vec{k}_2, j_2)$, which couples the resonant TO mode at $\vec{k} = 0$ (infrared photon momentum) to any two other modes with different indices j but with a combined momentum equal to zero or an integral number of reciprocal-lattice vectors, is given explicitly in Ref. 3. Following the procedure there which considered nearest neighbors only, it was found that $V^{(3)}$ could be written for the rocksalt structure:

$$V^{(3)}(0,j;\vec{k}, j_1; -\vec{k}, j_2) \propto [\omega(\vec{k}, j_1)\omega(-\vec{k}, j_2)]^{-1/2} \left[\phi''''(r_0)[m_x(\vec{k}, j_1|0)m_x(-\vec{k}, j_2|1) - m_x(\vec{k}, j_1|1)m_x(-\vec{k}, j_2|0)] \right]$$

$$\begin{aligned}
& + \frac{\phi''(r_0)}{r_0} \sum_{\alpha=y,z} [m_\alpha(\vec{k}, j_1 | 0) m_\alpha(-\vec{k}, j_2 | 1) - m_\alpha(\vec{k}, j_1 | 1) m_\alpha(-\vec{k}, j_2 | 0)] \sin(2\pi r_0 \vec{k} \cdot \vec{e}_\alpha) + \frac{\phi''(r_0)}{r_0} \\
& \quad \times \sum_{\delta=y,z} \left([m_\delta(\vec{k}, j_1 | 0) m_x(-\vec{k}, j_2 | 1) - m_\delta(\vec{k}, j_1 | 1) m_x(-\vec{k}, j_2 | 0) + m_x(\vec{k}, j_1 | 0) m_\delta(-\vec{k}, j_2 | 1) \right. \\
& \quad \left. - m_x(\vec{k}, j_1 | 1) m_\delta(-\vec{k}, j_2 | 0)] \sin(-2\pi r_0 \vec{k} \cdot \vec{e}_\delta) \right) \Big], \quad (7)
\end{aligned}$$

where $\phi''(r_0)$ and $\phi'''(r_0)$ are the second and third derivatives of the lattice potential energy, $m_\alpha(\vec{k}, j | K)$ is the α component of the Karo and Hardy normalized eigenvector for the K th-type ion in the mode \vec{k}, j , \vec{e}_α is a unit vector along the α coordinate and r_0 is the lattice constant. The reciprocal-lattice vector \vec{G} has been taken equal to zero in all cases thus making the cosine term in Eq. (18) of Ref. 3 equal to one. This cosine term became -1 only in the case of some boundary phonons when, according to Johnson and Bell $\vec{G} \neq 0$, and such a procedure was found unnecessary at least in the $\phi'''(r_0)$ coefficient of Eq. (7) which will be shown in Sec. IV to play the predominant role.

The potential derivatives were obtained by assuming a potential of the form

$$\phi(r) = -Ae^2/r + 6Ce^{-r/\rho}, \quad (8)$$

where A is the Madelung constant. C and the screening radius ρ are constants derived from the experimental measurement of the compressibility. The long-range Coulomb potential has been included since it reduces the second differential by 25% while reducing the third by only 9%. Since the theoretical values are to be scaled, it is only the ratio $\phi''(r_0)/r_0\phi'''(r_0)$ that is important. The constants used in Eq. (8) may be seen in Table I.

The lattice-dynamical data, kindly supplied by A. M. Karo, were obtained from a deformation-dipole model incorporating next-nearest-neighbor interactions and angle-bending forces, which has been applied to LiH and LiD.¹⁷ The data were for LiF at 0°K, thus making renormalization to harmonic frequencies unnecessary but introducing errors when applied to data obtained at higher temperatures. The data comprised eigenvalues and eigenvectors for the irreducible $\frac{1}{48}$ th of the Brillouin zone with a wave-vector density of 64 000 per zone. This gave, for example, 20 evenly spaced \vec{k} values from the origin to the $\langle 100 \rangle$ zone boundary. σ (summation) and α (difference) were calculated, making full use of the symmetry properties of each phonon mode, on an IBM 360/67 which took approximately 1 min for either one over the full frequency range. The Dirac δ functions in Eq. (5) allow σ and α to be calculated only at discrete values, which even with the high wave-vector density being used, can be spaced up to 20 cm^{-1} apart in

certain regions. A "bin-sampling technique" described by Caldwell and Klein¹⁸ was therefore used to smooth the data, the bin sizes being 20 cm^{-1} in the difference region and 10 cm^{-1} in the summation region. It is thought that the fine structure obtained by Ipatova *et al.*¹¹ was due to the lack of such a procedure.

IV. RESULTS

It will be more instructive if the summation region is considered first. The results of the present conductivity calculations are shown in Fig. 1, where the scaling factor has been taken from the difference measurements (see Sec. IV B). Also shown are the calculated results obtained when $\phi''(r_0)$ is set equal to zero. In Table I it may be seen that $\phi''(r_0)/r_0\phi'''(r_0)$ is only about 10%. Figure 1 demonstrates that the structure is largely determined by the density of states and the $\phi'''(r_0)$ coefficient. Of note also is the small overlap in wave number of the two types of processes. When the cubic coupling coefficient is assumed equal for all modes of different branch index j , as is done in combined density-of-states calculations as those of Dolling *et al.*,¹² not only is there too much structure, but the summation absorption extends far in-

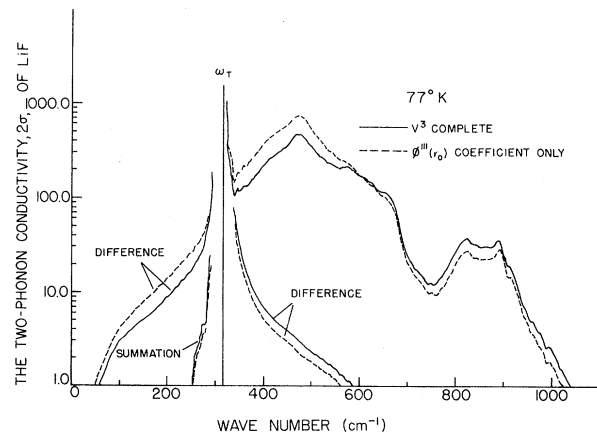


FIG. 1. Calculated two-phonon difference and summation conductivity of LiF, showing the frequency overlap of the two kinds of process and the effect of neglecting $\phi''(r_0)$ coefficients in the cubic coupling coefficient (scale determined experimentally).

TABLE I. Constants used to calculate the absorption constant α and conductivity σ for LiF.

Resonant absorption frequency ^a at 300 °K	ω_T	305 cm ⁻¹
Resonant absorption frequency ^a between 63 and 100 °K	ω_T	315 cm ⁻¹
Static dielectric constant at 300 °K	ϵ_0	9.0
Static dielectric constant between ^a 63 and 100 °K	ϵ_0	8.6
High-frequency dielectric constant ^a (all temperatures)	ϵ_∞	1.93
Madelung constant	A	1.748
Electron charge	e	4.8×10^{-10} esu
Screening radius ^b	ρ	0.244×10^{-8} cm
Lattice constant ^b	r_0	2.01×10^{-8} cm
Repulsive potential constant ^b	C	1.05×10^{-9} erg
Second derivative of potential	$\phi''(r_0)/r_0$	15.38×10^{12} erg cm ⁻³
Third derivative of potential	$\phi'''(r_0)$	-152.50×10^{12} erg cm ⁻³

^aSee Ref. 16.^bSee Ref. 19.

to the low-wave-number region with predicted values higher than for the difference absorption. In other words, the coupling between the low-frequency acoustic modes is far too high.

A. Summation Results

In Fig. 2 may be seen the experimental conductivity measurements² and the present calculations for the summation processes. The subsidiary maxima referred to in Ref. 2 are indicated by dashed arrows, whereas full arrows show the present theoretical maxima. Before suggesting the two phonon assignments for these maxima, it is instructive to refer to the phonon-dispersion curves of Karo and Hardy used in this calculation, which may be seen in Figs. 3 and 4. These curves together with selection rules inherent in the theory outlined allow an estimate to be made of which pairs combine strongly. There are three main criteria. First, for a summation band the two contributing phonon branches should have equal and opposite slopes. This gives a maximum in the combined density of states [see Eqs. (4) and (5)]. Second, the $\sin(2\pi r_0 \vec{k} \cdot \vec{e}_\alpha)$ -type terms in Eq. (7) are zero whenever $\vec{k}_\alpha = 0$ or $(2r_0)^{-1}$, e.g., \vec{k} at the point X equals $((2r_0)^{-1}, 0, 0)$. Finally from the eigenvectors in the $\phi'''(r_0)$ term it may be seen that combining modes must have at least one eigenvector component in the same direction²⁰ [i.e., the x direction in Eq. (7)] for the rocksalt structure. The intensity is enhanced if one of the eigenvectors is of opposite sign to the other three, producing a strong coupling between "normal" acoustic and optic modes. Not all symmetry modes are "normal" at all \vec{k} values, however, in as much as eigenvectors can change in nature from optic to acoustic across the zone. These guidelines do not contradict the selection rules obtained from group theory¹³ but go further in predicting the predomi-

nant features.

Along Δ , therefore, where group theory allows all possible combinations, the third consideration above leads to sizeable combinations of only $\Delta_1\Delta_2$ and $\Delta_5\Delta_5$ (the transverse modes have no eigenvector component in the same Cartesian direction as the longitudinal modes). The first consideration of opposite slopes rules out $\Delta_5\Delta_5$ leaving only $\Delta_1\Delta_1$. At X the second consideration of the sine term gives zero combinations in agreement with group theory. Between X and K the intensities will be low due again to the sine term, which is squared in Eq. (4). Along Σ the $(\text{sine})^2$ term will peak at 0.5, 0.5, 0, and so combinations should be looked for in this

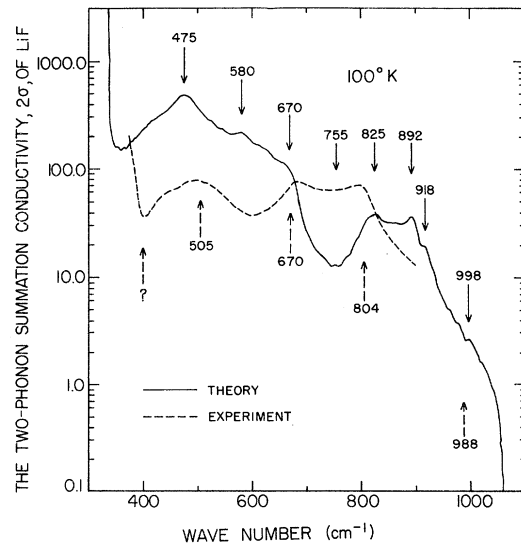


FIG. 2. Calculated two-phonon summation (corrected for overlap of difference processes) and experimental conductivity of LiF above the reststrahlen peak. Maxima in both are indicated.

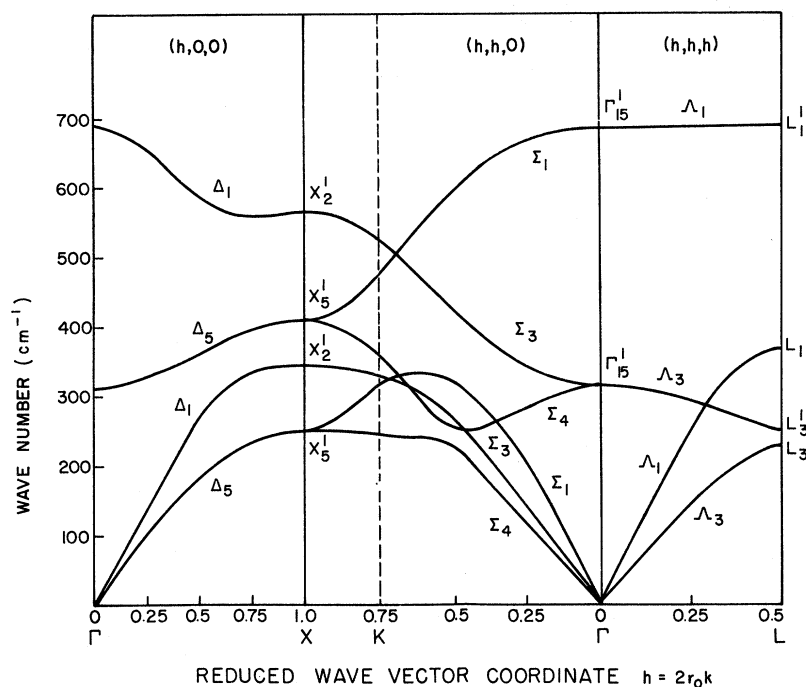


FIG. 3. Phonon-dispersion curves of LiF along the major symmetry directions, according to the modified deformation-dipole model of Karo and Hardy.

region. Σ_3 modes cannot combine with any others through the $\phi'''(r_0)$ term (see Table II where the $h=0.5, 0.5, 0$ eigenvectors are reproduced).

The $\Sigma_3\Sigma_3$ combination is disallowed since $k_x=0$. This leaves $\Sigma_1\Sigma_1$, $\Sigma_4\Sigma_4$ and all four combinations of $\Sigma_1\Sigma_4$. Two of these latter (LO:TO and LA:TA) might be expected to be small due to the predominant motion of the same ion in each, according to the Karo and Hardy eigenvectors. Since the

(sine)² term peaks at L , combinations along Λ will merge into maxima at L . In agreement with group theory, all combinations except $L'_1L'_3$ and L_1L_3 are allowed. These last two are forbidden since they both involve the entire motion of one ion only. Along Q all combinations are allowed but the density of states might be low. Along Z the intensity will be low since $k_x=(2r_0)^{-1}$ and $k_z=0$. At W the only possible combination through $\phi'''(r_0)$ from the

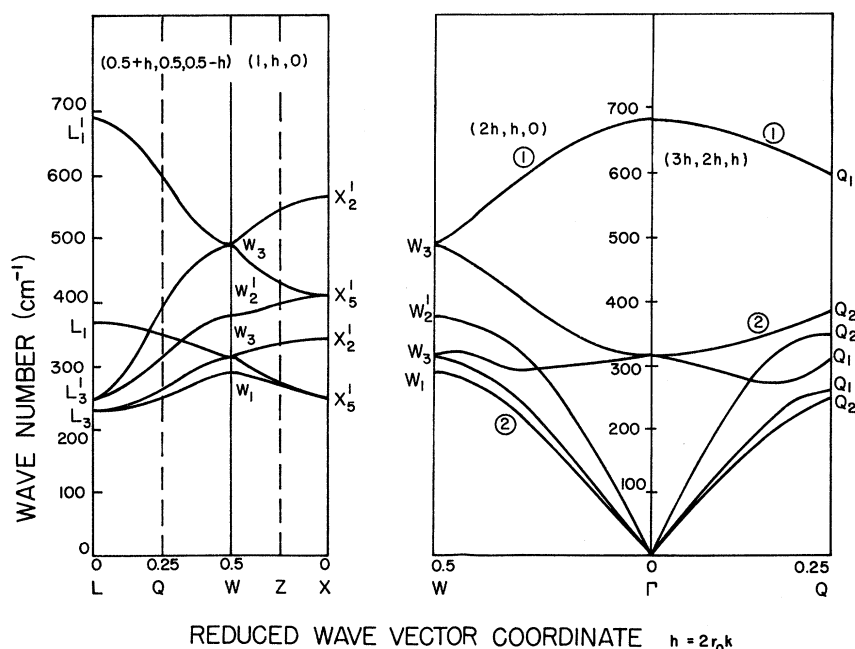


FIG. 4. Phonon-dispersion curves of LiF along less symmetrical directions, according to the modified deformation-dipole model of Karo and Hardy.

TABLE II. Eigenvectors for the mode with reduced-wave-vector coordinate equal to 0.5, 0.5, 0.

	$m_x(\text{Li}^+)$	$m_y(\text{Li}^+)$	$m_x(\text{Li}^-)$	$m_x(\text{F}^-)$	$m_y(\text{F}^-)$	$m_x(\text{F}^-)$
$\Sigma_1(\text{LO})$	0.676	0.676	0.0	-0.208	-0.208	0.0
$\Sigma_1(\text{LA})$	-0.208	-0.208	0.0	-0.676	-0.676	0.0
$\Sigma_3(\text{TO})$	0.0	0.0	0.973	0.0	0.0	-0.230
$\Sigma_4(\text{TO})$	-0.688	0.688	0.0	0.163	-0.163	0.0
$\Sigma_4(\text{TA})$	-0.163	0.163	0.0	-0.688	0.688	0.0
$\Sigma_3(\text{TA})$	0.0	0.0	0.230	0.0	0.0	0.973

Karo and Hardy eigenvectors is W_1W_2' . This completes the major symmetry directions where critical points are expected to produce maxima in the combined density of states.

Table III lists the arrowed features of the computed spectrum with the major contributing phonon pairs. Alongside are listed as far as possible the energies of the same phonon pairs as measured by neutron diffraction.¹² These values should be more accurate than the deformation-dipole data despite the temperature and isotopic difference. From the table it may be seen that the neutron values for L_3' , L_3 , $\Delta_1(\text{LO, near } X)$, and $\Delta_1(\text{LA, near } X)$ give much better agreement with experiment, while the W_2' and W_1 values may not be as good. (The position of the maximum has been taken as the point with greatest rate of change of slope.) The dip in the calculated curve around 750 cm^{-1} is due to the Karo-Hardy $\Sigma_1(\text{LO}) + \Sigma_4(\text{TA})$ combination occurring too high at 825 cm^{-1} and the lack of a dip around 580 cm^{-1} partly due to the $\Sigma_1(\text{LA}) + \Sigma_4(\text{TO and TA})$ combinations superimposing away from the neutron

predicted positions. The reason why the remaining predicted small features were not observed experimentally may be other frequency eigenvector discrepancies in the Karo-Hardy data.

A major point, which has been previously recognized and is reinforced here is the small part played by the usual critical points. This is due to several factors: the selection rule against overtones; the restricting effect of the sine term in Eq. (7) primarily along symmetry directions and at X ; the restriction of the $\phi'''(r_0)$ coupling coefficient acting primarily along symmetry directions. The usually high density of states arising from symmetry critical points is found to be rivaled by the high multiplicity of points with no symmetry (e.g., the multiplicity for any of the lowest symmetry points is 48, while that for the highest, at X , is 3). Consequently some of the smaller features of the computed spectrum are explained in Table II by low symmetry combinations, and the dispersion curves from Γ to W and Z have been included in Fig. 2 to show the contributing branches of nearly equal but opposite slopes. The large computed feature in I near 988 cm^{-1} is due to either $X_2'(0) + X_5'(0)$ or $L_1' + L_3'$, both of which are forbidden. The computed feature near 400 cm^{-1} is due to the two nondegenerate TA modes in the region around L_3 . These will not however combine strongly due to the predominant motion of one ion. It is now thought that the experimental feature seen there may be an isotope-induced one-phonon peak.²¹

Some probable symmetry combinations mentioned

TABLE III. A summary of the two-phonon summation absorption.

Energy of maxima produced by Karo-Hardy data ($\pm 2 \text{ cm}^{-1}$) in cm^{-1} .	Contributing phonon pairs (with energies in cm^{-1}) to the Karo-Hardy maxima.	Individual and combined energies of same phonon pairs using neutron dispersion data of Dolling <i>et al.</i> ^a	Experimental maxima ^b
475 (large)	$L_3'(246) + L_3(229)$ (large) $\Sigma_4(\sim 250) + \Sigma_4(\sim 225)$ (small)	$L_3'(295) + L_3(203) = 498$ $\Sigma_4(\sim 295) + \Sigma_4(\sim 193) = 488$	505
580 (medium)	$\Sigma_1(\text{LA}) + \Sigma_4(\text{TO})$ and $\Sigma_4(\text{TA})$ (large) $\Gamma \rightarrow Q$ (several contributions) (large)	$\Sigma_1(\text{LA} \sim 326) + \Sigma_4(\text{TO} \sim 300) = 626$ $+ \Sigma_4(\text{TA} \sim 200) = 526$	
670 (large)	$W_2'(380) + W_1(290)$ (large) Several combinations near Q (small)	$W_2'(379) + W_1(271) = 650$	670
755 (small)	Several combinations near Q		
825 (large)	$\Sigma_1(\text{LO} \sim 588) + \Sigma_4(\text{TA} \sim 237)$ (large) $\Gamma \rightarrow W$ (① and ②; see Fig. 4) (large)	$\Sigma_1(\text{LO} \sim 551) + \Sigma_4(\text{TA} \sim 193) = 744$	
892 (large)	$\Delta_1(\sim 560) + \Delta_1(\sim 332)$	$\Delta_1(\sim 454) + \Delta_1(\sim 348) = 802$	804
918 (small)	$\Sigma_1(\sim 594) + \Sigma_1(\sim 324)$	$\Sigma_1(\sim 546) + \Sigma_1(\sim 319) = 865$	
988 (small)	$\Gamma \rightarrow Q$ (① and ②; see Fig. 4)		988
1056 (limit of two-phonon absorption)	$L_1'(688) + L_1(368)$	$L_1'(623) + L_1(383) = 1006$	

^aSee Ref. 12.^bSee Ref. 2.

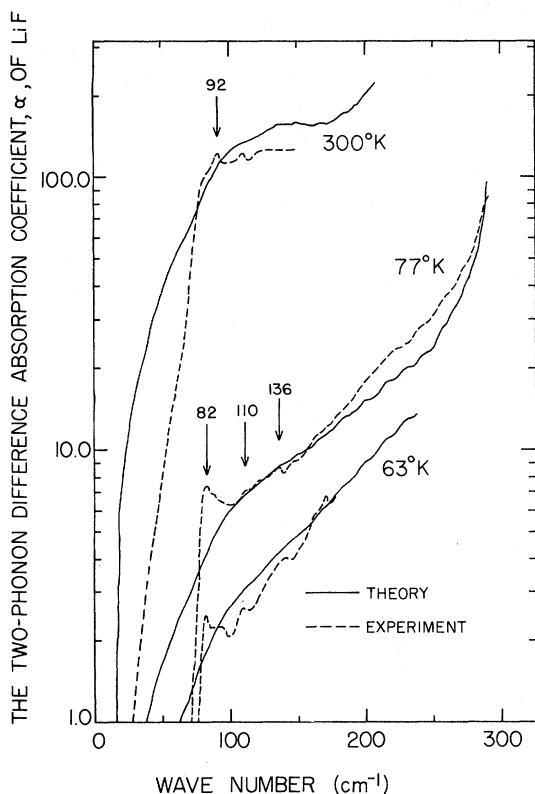


FIG. 5. Calculated two-phonon difference (corrected for overlap of summation processes) and experimental absorption coefficient of LiF below the reststrahlen peak. Experimental maxima are indicated (scaled by approximate fit of 77 °K data).

earlier but not seen in Table II are $\Sigma_1\Sigma_4(\text{LO TO})$, $L'_1 + L_3$, and $L_1 + L'_3$. All of these were found to be contributing but not sufficiently to create a maximum. $\Sigma_1\Sigma_4(\text{LO TO})$ was small around 840 cm^{-1} . $L'_3 + L_1$ peaked around 615 cm^{-1} , but this contribution was dwarfed by the large intensity from the Γ to Q and W branches culminating in the $W_1 + W'_2$ maximum. L'_1 plus L_3 was a minor contributor at 920 cm^{-1} . Thus it may be seen that high resolution combined densities-of-states curves like that of Dolling *et al.* are not too helpful.

B. Difference Results

In Fig. 5 may be seen plotted the values of the absorption coefficient measured in the far infrared according to Sec. II. The 77 °K values were measured to within about 20 cm^{-1} of the reststrahlen peak, while the values at 300 and 63 °K were measured only in the low-energy region where three-phonon processes might be expected to contribute in greater proportion. The value of α was obtained from the transmitted intensity with the sample in the beam, I_s , and out of the beam, I_R (reference) from the relation

$$\frac{I_s(\omega)}{I_R(\omega)} = \frac{(1-R)^2 e^{-\alpha d}}{1-R^2 e^{-2\alpha d}}, \quad (9)$$

where d is the mean sample thickness, and R the reflectivity, calculated from

$$R = \left(\frac{n-1}{n+1}\right)^2 \quad (10)$$

since k , the extinction coefficient, is small compared to n in this region. The refractive index was in turn calculated from a classical oscillator model,

$$n^2 = \epsilon_\infty + \frac{\epsilon_0 - \epsilon_\infty}{1 - \omega^2/\omega_T^2}. \quad (11)$$

The values of the constants in (11) were taken from Lowndes and Martin¹⁶ and interpolated for different temperatures. They may be seen in Table I. Such reflectivity values agree well with measurements made with 12° incident radiation. Equation (9) assumes an averaging over the multiple reflections inside the wedge-shaped sample.

The solid curves are the theoretical calculations of Sec. III for the difference processes. These have been scaled by approximately fitting the 77 °K data.

The good agreement in the temperature variation indicates that there appears little need to consider three-phonon processes, at least in the case of LiF at low energies and up to 300 °K. Higher temperatures are presumably needed. Figure 6 shows a similar graph to those plotted by Stolen and Dransfield,¹⁴ where the ratio of the two-phonon absorption constant α , predicted by the Karo-Hardy data, to temperature T is plotted versus T . In the high- T limit, the two-phonon processes should yield a straight horizontal line and any slope in the experimental curves will indicate the presence of three-phonon absorption. It is seen however that LiF is sufficiently hard (high frequencies) that

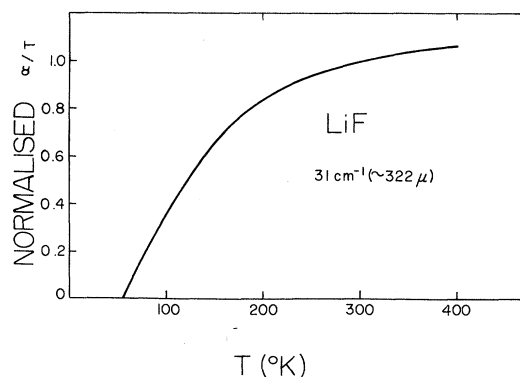


FIG. 6. Calculated two-phonon difference absorption coefficient of LiF at 31 cm^{-1} divided by absolute temperature, vs temperature. α/T is normalized to 1 at 300 °K.

two-phonon absorption is still not directly proportional to T by 300 or 400 °K. Another point concerning Ref. 14 is that the method of correcting for reflectivity is not clear and the value of α for LiF at 300 °K and 320μ (31 cm^{-1}) reported here is $1.7 \pm 0.3 \text{ cm}^{-1}$ compared with their value of 3.4 cm^{-1} (the reflectivity loss at 31 cm^{-1} is around 50%).

The lack of structure and the low-energy absorption predicted by the theory in Fig. 5 is again due to discrepancies in the Karo-Hardy frequencies. Upon inspecting the neutron-measured curves¹² again, one may see that the $82 \pm 2\text{-cm}^{-1}$ peak is due to either the L'_3L_3 difference ($\sim 92 \text{ cm}^{-1}$) or the $\Sigma_4\Sigma_4$ ($\sim 80 \text{ cm}^{-1}$) difference (near reduced wave-vector coordinate 0.6). At these points the slopes are parallel, a necessary condition for a high difference density of states, as opposed to the summation case, whereas in Fig. 3 the branches concerned are seen to approach each other, thereby producing no maximum but instead absorption extending to lower energy. The 92-cm^{-1} peak at 300 °K may be this same absorption with a net shift in frequency due to a greater anharmonic effect in one branch than the other, or perhaps the following may be the case. The neutron-measured point L_3 is about 20 cm^{-1} lower in energy than the lower Σ_4 branch. Now another consideration in the difference absorption as opposed to the summation is the fact that major contributions will, at "low" temperatures, come from only those pairs which involve one branch of the lowest possible energy, which has therefore the highest occupation. Taking the α values for the 82-cm^{-1} inflection at 300 °K, and peaks at 77 and 63 °K together with the 92-cm^{-1} values, and using the temperature dependence of Eq. (5b) the lower branch contributing to the 82-cm^{-1} peak is found to be 30 cm^{-1} , below the 92-cm^{-1} lower branch. This may indicate therefore the L'_3L_3 difference at 82 cm^{-1} and the $\Sigma_4\Sigma_4$ at 92 cm^{-1} . The maximum at 110 cm^{-1} is most likely due to $\Delta_5\Delta_5$ around $h=0.75$, and that at 136 cm^{-1} possibly due to $\Sigma_1(\text{LA})\Sigma_4(\text{TA})$. No other combinations along the symmetry directions seem likely to yield a maximum. Some nonsymmetry directions may have parallel pairs.

The 20-cm^{-1} bin size used in the difference calculation lost some of the structure present, yet

even so was not sufficient to smooth out the regular sampling ripples seen between 200 and 250 cm^{-1} where the difference density of states is low.

V. CONCLUSION

The features of the experimental conductivity of LiF above and below the reststrahlen peak have been explained in terms of specific two-phonon processes. The criteria used in predicting strong coupling between any two-phonon branches are slope matching, eigenvector considerations, and a $\sin(2\pi r_0 \vec{k} \cdot \vec{e}_\alpha)$ term that appears in the coupling coefficient. Occupation numbers must also be considered in the difference processes. These criteria supplement the selection rules derived from group theory. Some small features are found to be due to phonon branches with fortuitous slope matching along nonsymmetry directions.

Little evidence has been found for the presence of three-phonon processes at very low energies up to 300 °K in LiF. Early measurements⁶ have reported low three-phonon absorption at very high energies beyond the two-phonon limit.

The frequencies of the Karo and Hardy modified deformation-dipole model, used in these calculations, are found to differ appreciably from the more accurate neutron-measured values. Better agreement in the over-all conductivity spectrum could therefore be obtained by (i) using a model with improved frequencies and (ii) correct treatment of the denominator in Eq. (2). The reliability of the eigenvectors of such models is of course also unknown and finally one may question the accuracy of the real part of the refractive index, measured by reflectivity and a Kramers-Kronig analysis and used to obtain the experimental conductivity.²

As far as the agreement allows, one may note that the anharmonic mechanism alone seems satisfactory. More accurate measurements at high energies with knowledge of the multiphonon processes would be required to test this.

ACKNOWLEDGMENT

The author wishes to thank Professor A. M. Karo for kindly providing the lattice-dynamical data.

†Work supported in part by a grant from the National Research Council of Canada and in part by Grant No. 9510-35 from the Defense Research Board of Canada.

¹M. Gottlieb, *J. Opt. Soc. Am.* **50**, 343 (1960).

²A. M. Karo, J. R. Hardy, C. Smart, and G. P. Wilkinson, in *Lattice Dynamics*, edited by R. F. Wallis (Pergamon, New York, 1965), p. 387.

³K. W. Johnson and E. E. Bell, *Phys. Rev.* **187**, 1044 (1969).

⁴B. Szigeti, *Proc. Roy. Soc. (London)* **A258**, 377 (1960).

⁵R. A. Cowley, *Advan. Phys.* **12**, 421 (1963).

⁶V. V. Mitskevich, *Fiz. Tverd. Tela* **4**, 3035 (1962) [*Sov. Phys. Solid State* **4**, 2224 (1963)].

⁷A. M. Karo and J. R. Hardy, *Phys. Rev.* **129**, 2024 (1963).

⁸F. A. Johnson, *Progr. Semicond.* **9**, 181 (1965).

⁹J. R. Hardy and S. D. Smith, *Phil. Mag.* **6**, 1163 (1961).

¹⁰K. D. Möller and W. G. Rothschild, *Far Infrared Spectroscopy* (Wiley-Interscience, New York, 1971),

Chap. 12.

¹¹I. P. Ipatova, A. A. Maradudin, and R. F. Wallis, *Phys. Rev.* **155**, 882 (1967).

¹²G. Dolling, H. G. Smith, R. M. Nicklow, P. R. Vijayaraghavan, and M. K. Wilkinson, *Phys. Rev.* **168**, 970 (1968).

¹³E. Burstein, F. A. Johnson, and R. Loudon, *Phys. Rev.* **139**, 1239 (1965).

¹⁴R. Stolen and K. Dransfield, *Phys. Rev.* **139**, 1295 (1965).

¹⁵A. Hadni, in *Far Infrared Properties of Solids*, edited by S. S. Mitra and S. Nudelman (Plenum, New York, 1970), p. 561.

¹⁶R. P. Lowndes and D. H. Martin, *Proc. Roy. Soc. (London)* **308**, 473 (1969).

¹⁷S. S. Jaswal and J. R. Hardy, in *Localized Excitations*

in *Solids*, edited by R. F. Wallis (Plenum, New York, 1968), p. 643.

¹⁸R. F. Caldwell and M. V. Klein, *Phys. Rev.* **158**, 851 (1967). This technique amounted to convoluting the theoretical points evenly spaced in wave number, with a symmetrical triangular function. A further improvement could be obtained by using a function which represents a least-squares fit to some order of polynomial.

¹⁹M. Born and K. Huang, *Dynamical Theory of Crystal Lattices* (Clarendon, London, 1968), p. 26.

²⁰The manifestation of this coupling rule in two-phonon difference absorption measurements led Stolen and Dransfield (Ref. 14) to state that longitudinal and transverse modes do not combine at all, whereas this is true only in a few cases.

²¹J. E. Eldridge, *Phys. Rev. B* (to be published).

PHYSICAL REVIEW B

VOLUME 6, NUMBER 4

15 AUGUST 1972

Energy-Band Structure of SrTiO₃ from a Self-Consistent-Field Tight-Binding Calculation*

Thomas F. Soules,[†] Edward J. Kelly, and David M. Vaught[‡]
Department of Chemistry, Purdue University, Lafayette, Indiana 47907

and

James W. Richardson
Department of Chemistry, Purdue University, Lafayette, Indiana 47907
and Philips Research Laboratories, Eindhoven, The Netherlands
 (Received 5 November 1971)

Energy bands of SrTiO₃ have been computed *ab initio* using a nonrelativistic self-consistent-field (SCF) procedure based upon the linear-combination-of-atomic-orbitals or tight-binding formalism. A slightly extended multicentered-atomic-orbital basis was used and integrals over them were evaluated in keeping with the Hartree-Fock-Roothaan procedures. Three- and four-centered integrals were treated by previously justified numerical approximations. Results are in good agreement with experimental evidence for the ordering and widths of the valence and conduction bands. A 12.1-eV band gap was obtained, however, from the ground-state SCF results. Consideration of various energy terms and comparison with an independent SCF calculation on the isolated TiO₆⁸ cluster confirm Šimánek and Šroubek's earlier criticism of Kahn and Leyendecker's semiempirical model and suggest significant hole-particle correlation in the electronically excited states of the crystal. Though by a less rigorous analysis, the Sr orbital interactions are judged not to perturb the features of these results.

I. INTRODUCTION

Over the past several years, numerous physical properties of SrTiO₃ and similar transition-metal oxides have been measured with recent interpretations of the electronic properties of SrTiO₃ based on the semiempirical band structure of Kahn and Leyendecker.^{1,2} Their calculated results were in good agreement with the experimental data then available although some discrepancies have since appeared.^{3,4}

Kahn and Leyendecker used an adjustable ionic model to represent the lattice-crystal-field potential. A completely ionic model predicts an energy gap of 17 eV separating the oxide 2*p* valence orbitals from the vacant titanium 3*d* orbitals. Their innovation was to attribute the observed

absorption edge at 3.2 eV to a departure from complete ionicity in the titanium-oxygen bond. Šimánek and Šroubek⁵ correctly criticized their implementation, however, since it neglects changes in the oxide and titanium ionization potentials concomitant with a transfer of charge from the oxygen to titanium atoms. These effects were estimated and found approximately to cancel the effect of the change in Madelung potential at the titanium and oxygen sites. Alternatively, then, to explain the apparent reduction in band gap, Šimánek and Šroubek propose a Heitler-London model for the excited state of the crystal in which the hole and electron are associated with neighboring oxygen and titanium ions, respectively. The transition energy is reduced by large hole-electron interaction and polarization effects on the surrounding